# Suitability of ground-based SfM-MVS for monitoring glacial and periglacial processes

**L. Piermattei[1], L. Carturan[1], F. de Blasi[1], P. Tarolli[1], G. Dalla Fontana[1], A. Vettore[2] and N. Pfeifer[3].**

[1]Department of Land, Environment, Agriculture and Forestry, University of Padova, Italy

[2]Interdepartment Research Center of Geomatics, University of Padova, Italy

[3]Department of Geodesy and Geoinformation, TU Wien, Austria

Correspondence to: L. Piermattei (livia.piermattei@studenti.unipd.it)

## Abstract

Photo-based surface reconstruction is rapidly emerging as an alternative survey technique to LiDAR (light detection and ranging) in many fields of geoscience fostered by the recent development of computer vision algorithms such as Structure from Motion (SfM) and dense image matching such as Multi-View Stereo (MVS). The objective of this work was to test the suitability of the ground-based SfM-MVS approach in calculating the geodetic mass balance of a 2.1 km$^2$ glacier and for the detection of the surface displacement rate of a neighbouring active rock glacier located in the Eastern Italian Alps. The photos were acquired in 2013 and 2014 using a digital consumer-grade camera, organizing single-day field surveys. Airborne laser scanning (ALS) data were used as benchmarks to estimate the accuracy of the photogrammetric digital elevation models (DEMs) and the reliability of the method. The SfM-MVS approach enabled the reconstruction of high-quality DEMs, which provided estimates of glacial and periglacial processes similar to those achievable by ALS. In stable bedrock areas outside the glacier, the mean and the standard deviation of the elevation difference between the SfM-MVS DEM and the ALS DEM was -0.42 m ± 1.72 m and 0.03 m ± 0.74 m in 2013 and 2014, respectively. In the rock glacier area, the elevation difference was 0.02 m ± 0.17 m. The use of natural targets as ground control points, the occurrence of shadowed and low-contrast areas, and in particular the sub-optimal camera network geometry imposed by the morphology of the study area were the main factors affecting the accuracy of photogrammetric DEMs.

## 1. Introduction

Knowledge of changes in the extent, mass and surface velocity of glaciers and rock glaciers contributes to better understanding the dynamic processes occurring in cold high-mountain environments and serves as an important contribution to climate monitoring (Kääb et al., 2003).

Numerous techniques exist for monitoring and quantifying these changes and include both field and remote sensing methods (Immerzeel et al., 2014). Fieldwork generally yields high-quality data but with a small spatial extent, given the remoteness and low accessibility of mountain areas at high elevations (Roer et al., 2007). Therefore, using remotely sensed datasets for at least two different points in time has become an important tool for monitoring high-mountain terrain dynamics (Kääb, 2002). Multitemporal Digital Elevation Models (DEMs) based on remote sensing data are the most commonly used products for such investigations (Kääb, 2005; Tseng et al., 2015).

Among the available remote sensing techniques, the close-range photogrammetry saw a rapid development thanks to the recent evolution of digital photogrammetry, based on computer vision algorithms. This technique is becoming the major alternative to traditional surveying techniques and LiDAR (light detection and ranging) technologies, due to its lower cost, high portability, and easy and rapid surveying in the field.

The photogrammetric approach known as Structure from Motion (SfM) allows obtaining 3D information of the photographed object from a sequence of overlapping images taken with a digital camera.

A limited number of applications of SfM photogrammetry in glacial and periglacial environments exists, and they principally involve the use of Unmanned Aerial Vehicles (UAVs) for image acquisition (Solbø S. and Storvold R. 2013; Whitehead et al., 2013; Immerzeel et al., 2014, Tonkin et al., 2014; Gauthier et al., 2014; Bühler et al., 2014; Dall'Asta et al., 2015; Ryan et al., 2015) rather than ground-based surveys (Gómez-Gutiérrez et al., 2014; 2015; Kääb et al., 2014; Piermattei et al., 2015).

The objective of our work was to assess the suitability of the ground-based SfM approach for monitoring glacial and periglacial processes in a high-altitude area of the Ortles-Cevedale Group (Eastern Italian Alps). In particular, this approach was used to calculate the geodetic annual mass balance of a 2.1 $km^2$ glacier and to detect the surface displacement of a neighbouring 0.06 $km^2$ rock glacier. The

photogrammetric surveys were intentionally planned to be as quick and cost-effective as possible, and easily replicable in the future. Therefore, a consumer-grade camera was adopted to find an appropriate balance between the affordability and accessibility of the system (i.e. cost and ease of use) and the quality of the resulting topographic data (accuracy and density). The accuracy of the photogrammetric DEMs was estimated using ALS-based DEMs acquired during the same periods. The main factors affecting the accuracy of the photogrammetric DEMs were investigated, and the significance of the biases in the quantification of glacial and periglacial processes was discussed.

## 2. Geographical setting and case studies

The La Mare Glacier and the neighbouring AVDM3 Rock Glacier are located in the south-eastern part of the Ortles-Cevedale massif (Eastern Italian Alps), the largest glaciated mountain group of the Italian Alps (Fig. 1).

The La Mare Glacier (World Glacier Inventory code I4L00102517; WGMS 1989) is a 3.55 $km^2$ valley glacier currently composed of two ice bodies, which have different morphologies and tend to separate (Carturan et al., 2014). In this work, the focus was on the southern ice body, which feeds the main tongue. This 2.1 $km^2$ ice body primarily faces north-east, and its surface is rather flat, with the exception of the small remnant of its valley tongue. The elevation ranges from 2660 to 3590 m a.s.l. Mass balance investigations using the direct glaciological method were started on La Mare Glacier in 2003 and detected an average annual mass balance of -0.76 m w.e. $y^{-1}$ during the period from 2003 to 2014 (Carturan, 2016). The mass balance was close to zero in 2013 (-0.06 m w.e.) and was positive for the first time since the beginning of measurements in 2014 (+0.83 m w.e.).

The AVDM3 Rock Glacier (Carturan et al., 2015) is an intact, tongue-shaped rock glacier characterized by the presence of two lobes. The 0.058 $km^2$ wide Rock Glacier (maximum length of 390 m; maximum width of 240 m) faces south-east and is located at elevations of between 2943 and 3085 m a.s.l. The average slope of the Rock Glacier is 26°, and the slope of the advancing front is 36°. The activity status of the AVDM3 Rock Glacier was assessed via repeated geomorphological field surveys between 2007 and 2014. These surveys revealed the advance of the front of the southern lobe (Carturan, 2010). The general morphology and the elevation of the

front also suggest that this rock glacier is active (Seppi et al., 2012), and its permafrost content is further corroborated by spring temperature measurements (Carturan et al., 2015). Moreover, Bertone (2014) provided the first quantification of the surface displacement rates of this rock glacier for 2003 to 2013 using ALS data.

## 3. Methods

### 3.1 The ALS data

ALS flights of the study area were available for 17 September 2003, 22 September 2013, and 24 September 2014. The technical specifications of the three ALS surveys are reported in Table 1. To avoid errors due to global shifts or rotations between the individual DEMs, the ALS point clouds were automatically co-registered using a version of the ICP algorithm (Chen and Medioni, 1991; Besl and McKay, 1992) tailored to topographic point clouds (Glira et al., 2015). The LiDAR point cloud acquired in 2013 was treated as a reference only for stable areas outside the glaciers, rock glaciers, snow patches, and geomorphologically active areas (e.g., landslides, river beds, and debris flows). The 2003 and 2014 LiDAR point clouds were iteratively fitted to the reference point cloud by applying an affine transformation. The ICP registration of the point clouds produced z-direction residual values of 0.08 m and 0.11 m for the 2014 and 2003 LiDAR point clouds, respectively. These accuracies can be assumed to be sufficient for calculating the annual elevation changes of the glacier and the decadal displacement rate on the rock glacier.

The co-registered point clouds were then converted to DEMs using Natural Neighbours interpolations. A pixel size of 1 x 1 m was produced for the La Mare Glacier, whereas a pixel size of 0.5 x 0.5 m was used for the rock glacier, based on the LiDAR point cloud density (Fig. 2). To evaluate the relative ALS DEM accuracies after the co-registration, the elevation difference errors of the DEMs were calculated for the stable areas. The standard deviation from the 2013 ALS DEM was 0.19 m and 0.21 m for the 2014 and 2003 DEM comparisons, respectively.

## 3.2 The photogrammetric workflow

### 3.2.1 Field surveys

The terrestrial photogrammetric surveys of the La Mare Glacier were conducted on 4 September 2013 and 27 September 2014, that is, close to the end of the mass balance year and of ALS flights. The timing of the surveys enabled the calculation of the annual mass balance of the glacier and to compare the results with the ALS-based results. On both days, the sky was clear, with almost no cloud cover.

To guarantee a safe and easily repeatable survey of the glacier, the direct access to its surface was avoided and the survey was performed from a rocky ridge on the north side of the glacier (Fig. 5). The elevation of the survey ranged from 3100 to 3300 m in 2013 and from 2600 to 3300 m in 2014. The distance from the glacier surface to the camera positions dictated by the topography ranged between 300 and 2900 m. To cover the entire glacier surface from these positions, the acquired images were panoramic, which involved taking a series of photographs rotating the camera from each individual camera position. In 2013, seven camera positions were used, and 37 photographs were taken with the camera attached to a small tripod to avoid camera shake. In 2014, the number of camera positions was increased to 21, and 177 photos were taken freehand (Fig. 3).

Both surveys were performed using a SLR Canon EOS 600D. The camera was equipped with a 25-70 mm zoom lens, which was set to a focal length of 25 mm in 2013 and 35 mm in 2014.

The terrestrial photogrammetric survey of the AVDM3 Rock Glacier was performed on 27 September 2014. In this survey, 198 images were acquired freehand while walking around and on top of the rock glacier. The survey camera was a CANON EOS 5D full frame SLR camera equipped with a fixed-focal lens of 28 mm. The photographs were acquired and saved in RAW format in both surveys.

### 3.2.2 Data processing

The latest evolution of photogrammetry is characterized by the combination of the principles of photogrammetry, such as bundle adjustment, and automatic computer vision algorithms, such as feature extraction and feature matching. This photogrammetric approach, called Structure from Motion (SfM), can automatically

derive the 3D position of an object in images taken in sequence calculating the camera parameters (intrinsic and extrinsic) (Hartley and Zissermann, 2004). Dense image matching algorithms are then used to reconstruct the 3D model of the object as a dense point cloud. Multiple photogrammetric packages implementing SfM and Multi-View Stereo (MVS) algorithms for dense image matching exist, and in this work, the software PhotoScan Pro (AgiSoft LLC. 2010a) was used. Henceforth, the photogrammetric surveys and results are referred to using the acronym SfM-MVS.

The photo-based reconstruction workflow is summarized in Fig. 4. The key components of the workflow are 1) acquisition and photograph editing, 2) GCPs identification, image feature detection, matching and 3D scene reproduction (the SfM-MVS steps), 3) point cloud processing, (filtering, subsampling and ICP) and 4) DEM reconstruction.

To overcome the significant variability in brightness during the surveys, the RAW images have been edited to adjust the exposure and contrast in order to retrieve information from the overexposed (e.g., snow-covered) areas and underexposed (e.g., shadowed) areas. These editing steps had a positive impact on the number of image features extracted. The edited images were saved in TIFF format and loaded in PhotoScan where non-stationary objects (i.e., clouds and shadows), the sky, and features lying in the distant background have been masked.

The camera calibration parameters were calculated using artificial targets prior to the processing of the photogrammetric surveys (pre-calibrated camera). The intrinsic parameters were kept constant during the entire SfM processing given the limits of the camera network geometry and the homogeneous texture of the surveyed terrain. As additional constraint, the GCPs were included into the SfM process to avoid instability in the bundle adjustment solution (Verhoeven et al., 2015). The GCPs were selected as natural features in stable area outside the glacier and rock glacier, and their coordinates were extracted from the 2013 ALS hillshaded DEM. After the SfM step, the geo-referenced dense point cloud was reconstructed by the MVS algorithm, using the ‘mild’ smoothing filter to preserve as much spatial information as possible (AgiSoft LLC., 2010b).

To reduce the noise and outliers generated during the dense matching reconstruction (Bradley et al., 2008; Nilosek et al., 2012), an initial filtering was performed in PhotoScan to manually remove the outliers. Further denoising was applied to the dense point clouds exported from PhotoScan, using a specific tool to treat the point

clouds. To obtain a uniform spatial distribution of the points, the photogrammetric point clouds (much denser than the ALS point clouds), were down-sampled to 20 cm for the glacier and 10 cm for the rock glacier. Following the same procedure used for the ALS data, the ICP algorithm (OpalsICP, TU Wien) was applied to co-register the point clouds in the stable area outside the glacier and rock glacier, using the 2013 ALS point cloud as a reference. The co-registered point clouds were then converted to DEMs, using the Natural Neighbours interpolation and the pixel sizes of the ALS DEMs (i.e., 1 x 1 m for the glacier and 0.5 x 0.5 m for the rock glacier). The data acquisition settings and processing results of the photogrammetric surveys are summarized in Table 2.

### 3.3 Analyses

The accuracy of the photogrammetric DEMs was assessed calculating the mean, the mean of the absolute values and the standard deviation (σ) of the elevation differences (DEM of Difference, DoD) between SfM-MVS DEMs and ALS DEMs, using the latter as a reference dataset. For both surveyed areas, the primary factors controlling the quality of the photogrammetric results (i.e., camera–object distance, slope and angle of incidence, camera network geometry, surface texture and shadows) were evaluated in terms of DEM accuracy and spatial resolution. The obtained results were compared to the theoretical behaviour of the error as a function of the depth ($\sigma_d$), calculated using the following formulation:

$$\sigma_d = m_B \cdot \frac{D}{B} \cdot \sigma_i, \quad (1)$$

where $m_B$ represents the image scale (*D / focal length*); *D* is the depth (camera-object distance); B is the baseline and $\sigma_i$ is the measured accuracy in the image space.

After the accuracy assessments, we investigated the suitability of using the terrestrial photogrammetric surveys to calculate the annual mass balance of the glacier and the surface displacement rates of the rock glacier, comparing the results with those obtained from ALS surveys. The mass balance and elevation changes were calculated differencing multitemporal DEMs.

The geodetic mass balance was calculated from the total volume change ΔV ($m^3$) between two survey dates:

$$V = \overline{\Delta z} \cdot A \quad (2)$$

where $\overline{\Delta z}$ is the average elevation change between two DEMs over the area *A* of the glacier. The area-averaged net geodetic mass balance in metres of water equivalent per year (m w.e. $y^{-1}$) was calculated as:

$$\dot{M} = \frac{\Delta V \cdot \rho}{A} \quad (3)$$

where $\rho$ is the mean density. The area *A* of the glacier between the two surveys did not change. The mean density was obtained by a fractional area-weighted mean, assigning 900 kg/$m^3$ for the ablation area (Huss, 2013) and 530 kg/$m^3$ for the accumulation area, as directly measured in a snowpit. The resulting weighted mean density was 600 kg/$m^3$. In the mass balance calculations, both raw $\overline{\Delta z}$ values and corrected $\overline{\Delta z}$ values were used to account for the mean errors in the stable areas outside the glacier, as reported in Table 3. Other processes like ice fluxes, varying snow density and re-freezing of melt water were assumed to be negligible for the calculation of the annual geodetic mass balance (Zemp et al., 2013).

The horizontal surface displacements rates of the AVDM3 rock glacier were estimated by a manual measurement of the displacement of single boulders identified in the hillshaded DEMs. Several points were also located outside the rock glacier to assess the accuracy of the surface velocity determinations. Displacements in the horizontal plane were analysed instead of 3D displacements, which are affected by surface elevation changes (Isaksen et al., 2000).

## 4. Results

### 4.1 Accuracy assessment on the area of La Mare Glacier

The mean elevation difference between the SfM-MVS DEM from 4 September 2013 (Fig. 5a) and the ALS DEM from 22 September 2013 (Fig. 2b), evaluated in the common stable area outside the glacier, was -0.42 m (σ = 1.72 m). The same calculation between the SfM-MVS DEM from 27 September 2014 (Fig. 5b) and the ALS DEM from 24 September 2014 (Fig. 2a) yielded a mean value of 0.03 m (σ = 0.74 m). In this area, the mean difference between the 2014 and 2013 SfM-MVS DEMs is 0.38 m (σ = 1.73 m), and the mean difference between the respective ALS DEMs is -0.09 m (σ = 0.29 m, Table 3).

These results show that the photogrammetric survey conducted in 2014, using a higher number of camera positions and photographs and a slightly longer focal length, provided a significant improvement compared to the survey of 2013. In addition to the higher σ, the 2013 SfM-MVS DEM has a residual average bias of -0.42 m, which must be taken into account in the glacier mass balance calculations. Table 3 presents the same statistics for the area of the glacier. However, given that in 2013 the ablation was not negligible between the photogrammetric survey of 4 September and the ALS survey of 22 September, the comparison between SfM-MVS and ALS of the same year is meaningful only in 2014, with a mean difference of 0.23 m (σ = 0.65 m). The comparison of the two ALS DEMs of 2014 and 2013 yields a mean difference of 1.30 m for the glacier, attributable to the positive mass balance experienced by the glacier in that time period (+0.83 m w.e., Carturan, 2016).

The spatial distribution of the elevation difference between the SfM-MVS and ALS DEMs surveyed at the same times (Fig. 6 and 7) suggests that the most problematic areas for photogrammetric reconstructions are those that are far from the camera positions, steep, and covered by fresh snow. Certain outliers can be observed in steep areas outside the glaciers, even after filtering, but they likely have no influence on the glacier, where the slope is much lower.

The factors controlling the quality of the photogrammetric DEMs were investigated in detail using the SfM-MVS DEM from 27 September 2014, which has a higher spatial coverage than that of 2013 and is almost contemporaneous with the ALS DEM from 24 September 2014 (which means negligible ablation and accumulation on the glacier).

As expected, the standard deviation of elevation differences between the 2014 SfM-MVS and ALS DEMs is proportional to slope but remains lower than 1 m up to 40° on the glacier and up to 60° in the area outside it (Fig. 8). Grouping the data for slope classes of 10 degrees and excluding classes with less than 1000 grid cells, it was possible to calculate a strong correlation between the absolute value of the elevation difference and the slope (R = 0.86 both inside and outside the glacier, significant at the 0.05 level). A rapid increase in the error is observed for the highest slope classes, which represent a very small part of the investigated area. For the glacier, only 1% of the area has a slope higher than 40°. The mean elevation difference is around zero for most of the low- and middle-slope classes, with the exception of the 0-10° class inside the glacier, where a mean value of 0.41 m (σ = 0.44 m) was calculated.

Interestingly, the majority of this slope class lies in a flat area of the glacier at 3200-3300 m a.s.l. and is covered by fresh snow, which has poor texture. In addition, this zone has an unfavourable line of sight from the camera positions.

The role of the incidence angle between the line of sight of the camera and the photographed object (vector normal to the surface), was investigated by analysing the mean angles calculated from five representative camera locations at different elevations. The analysis was performed for the glacier area, where most of the mean incidence angles ranges between 70° and 90° (75%, Figure 9a). The scatterplot of elevation differences between the 2014 SfM-MVS and ALS DEMs versus the mean incidence angles calculated for every pixel shows no statistically significant relationship (R = 0.21). However, by analysing this relationship for classes of incidence angle, and considering the mean of the elevation differences in absolute value and the classes with more than 1000 pixels, yields a correlation coefficient R = 0.95 (significant at the 0.05 level).

Because the redundancy of the observations, that is the number of cameras that views the same points on the glacier, influences the quality of the photogrammetric results, a viewshed analysis was carried out (Fig. 9d). The results show anti-correlation between the absolute value of elevation difference and the number of cameras viewing reconstructed pixels (Fig. 9e), yielding a coefficient of correlation of -0.63, which is significant at the 0.05 level.

The effect of the camera-object distance (i.e., depth, Gómez-Gutiérrez et al., 2014), was evaluated by calculating the mean and standard deviation of the elevation difference between the 2014 SfM-MVS and ALS DEMs, clustering the pixels in 200 m distance classes from a camera position at the centre of the array displayed in Figure 4b. The relationship between error and depth is clearer for the glacier area (Fig. 10a), whereas in the surrounding area, the error appears to be more influenced by the variability of the slope angle (Fig. 10b).

The theoretical $\sigma_d$ was calculated using Eq. 1 for each class of distance, considering a mean baseline of 400 m and an accuracy in the image space of 0.40 pixel, which is the reprojection error after bundle adjustment computations. Another quantification of the error as a function of the depth was obtained, for comparison purposes, by multiplying the Ground Sample Distance (GSD) (which increases with depth) by the reprojection error provided by PhotoScan for the Ground Control Points. Figure 10c shows that, on the glacier, the accuracy calculated from the DoD matches quite well

328 the ‘theoretical’ calculations up to a depth of 1900 m. Beyond this distance, the
329 detected error increases faster than in theory, likely due to the increasing coverage of
330 fresh snow, which affects the image texture and decreases the accuracy.
331 The accuracy of photogrammetric reconstructions for the different substrata was then
332 evaluated. The spatial distribution of each substratum was outlined on the orthophoto
333 exported from PhotoScan. Debris, ice and firn display similar accuracy, with median
334 values of elevation difference between the 2014 SfM-MVS and ALS-based DEMs
335 close to zero and interquartile ranges of the same magnitude. Conversely, the area
336 covered by fresh snow, which is also the area with greater depth, shows prevailing
337 positive differences, a median value of 0.48 m and a much higher standard deviation
338 ($\sigma$ = 0.82 m).
339 The texture of the surface also influences the point density distribution and the spatial
340 coverage of the reconstructed area. A lower value of the point density was obtained
341 for fresh snow (4 pts $m^{-2}$). Increasing point densities were obtained for firn, ice and
342 debris (10, 13 and 15 pts $m^{-2}$, respectively).
343 The spatial coverage in the fresh snow area was 75%, whereas it was 93% in the
344 rest of the glacier. Excluding the areas not visible from the camera position and
345 occlusions imposed by the topography, the spatial coverage in the fresh snow area
346 was 82% and 98% in the remaining part.
347 The point density is also affected by the depth, elevation and slope (Fig. 12). Due to
348 the GSD, the average point density decreases with depth, which in our case is also
349 proportional to the elevation. On the glacier, the point density decreases more rapidly
350 than in the surrounding area for elevations between 3100 and 3300 m a.s.l., due to
351 the poor texture in this snow-covered flat area. Increasing densities with slope, up to
352 70-80°, are observed and likely result from more favourable incidence angles, which
353 do not however guarantee high accuracy, as noted earlier (Fig. 9). Considering the
354 entire reconstructed surface, the point density was higher in the area surrounding the
355 glacier than on it (12 pts $m^{-2}$ vs. 8 pts $m^{-2}$, respectively).

356

357 **4.2 Accuracy assessment in the area of the AVDM3 Rock Glacier**

358 The 2014 terrestrial photogrammetric survey of the AVDM3 Rock Glacier provided a
359 good spatial coverage (83%) of high-resolution terrain data (Fig. 13). The spatial
360 distribution of the elevation difference between the contemporaneous SfM-MVS and

ALS DEMs shows the existence of areas with both positive and negative values (Fig. 14). The average elevation difference is 0.02 m on the rock glacier (σ = 0.17) and 0.05 in the surrounding areas (σ = 0.31 m, Tab. 5).

Similar to the La Mare Glacier area, the accuracy decreases with increasing slope in the rock glacier area. The standard deviation of the average elevation difference between the SfM-MVS and ALS DEMs is less than 0.20 m up to 40°. In the area surrounding the rock glacier, the error increases faster with slope because steep areas coincide with shaded areas and (because the images were acquired in the afternoon) high solar zenith angles. As suggested by Gómez-Gutiérrez et al., (2014), the relationship between the quality of the photogrammetric DEM and the amount of shadowed-lighted areas in the photographs was calculated using a hillshaded model that was calculated by simulating the position of the sun in the sky (azimuth and zenith angles) during the survey. As shown in Figure 16, larger errors occur in shadowed areas and smaller errors in well-lit areas, even if the largest differences in accuracy can be observed outside rather than on the rock glacier.

## 4.3 Glacial and periglacial processes

### 4.3.1 Mass balance of La Mare Glacier

Due to abundant solid precipitation during the accumulation season and low ablation rates during the summer (the glacier was snow-covered above ~3000-3100 m a.s.l.), the mass balance of the La Mare Glacier was positive in the 2013-14 hydrological year for the first time since the beginning of measurements in 2003. According to the direct glaciological method, the annual mass balance was +0.83 m w.e. (Carturan, 2016).

As shown in Table 4, the geodetic mass balance estimates using only ALS data do not differ significantly for either the entire glacier or the sub-areas covered by the photogrammetric surveys of 2013 and 2014 (88% and 93%, respectively). The estimates range between 0.85 and 0.88 m w.e for the raw data and between 0.90 and 0.94 m w.e. for the corrected data. The geodetic mass balance calculations using only photogrammetric data yield a raw value of 1.09 m w.e. and a corrected value of 0.87 m w.e. Using the 2014 SfM-MVS, which has a higher quality than the 2013 ALS DEM, yields a raw value of 0.98 m w.e. and a corrected value of 1.02 m

w.e. Area-averaged estimates of the geodetic mass balance from photogrammetric data are very close to the estimates from ALS data and from the direct method and are closer still if the mean DEM error in the stable areas outside the glacier is subtracted from the raw average elevation differences. The spatial distribution and magnitude of elevation change is also well captured by the terrestrial photogrammetry (Fig. 17 and 18), even if, as already noted in the previous section, problematic areas are present in the upper part of the glacier, which was covered by fresh snow, especially in the 2013 SfM-MVS survey.

### 4.3.2 Surface changes and velocities of the AVDM3 Rock Glacier

The spatial distribution and the mean value of elevation change on the surface of the AVDM3 Rock Glacier were calculated differencing the available SfM-MVS and ALS DEMs. Table 5 shows that, according to the ALS data, there was a prevailing lowering of the surface in the period from 2003 to 2014. Taking into account the average residual bias in the stable area outside the rock glacier, the average lowering rates of the rock glacier surface were 1.5 cm $y^{-1}$ in the period from 2003 to 2013, and 2 cm in the year 2013-14. Comparing the SfM-MVS DEM of 2014 with the ALS DEMs of 2013 and 2003 and accounting for the mean bias outside the rock glacier, we obtained slightly higher lowering rates of 2.2 cm $y^{-1}$ from 2003 to 2013 and 5 cm from 2013 to 2014. As expected on the basis of the accuracy assessment (Section 4.2), the decadal lowering rates calculated from the SfM-MVS DEM are in closer agreement with those calculated from ALS data than the single-year calculations. The same can be observed for the spatial distribution of the elevation changes (Fig. 19), which shows a prevailing thinning in the upper and middle part of the rock glacier and a thickening of the two advancing lobes. Figure 20 shows that the fastest moving areas in the period from 2003 to 2014 were the two frontal lobes, which also featured the greatest elevation changes. Table 6 shows that the SfM-MVS and ALS data produced very similar surface velocities for the three sub-areas (each with homogeneous displacement) into which the rock glacier can be divided. Outside the rock glacier, the photogrammetric method exhibited a slightly lower accuracy compared to the ALS, but no systematic shift of the different DEMs was found.

## 5. Discussion

### 5.1 Data processing and accuracy assessments

The results of our terrestrial photogrammetry applications on the La Mare Glacier and on the AVDM3 Rock Glacier demonstrate that it is possible to reliably quantify the investigated glacial and periglacial processes by means of a quick and safe survey that was conducted on a single day using cheap, light and easy-to-use hardware. Moreover, time-consuming and unsafe direct access to the glacier surface was not required.

The data processing times were significantly long. For a single operator, the processing time is approximately 10 days. The most labour-intensive and time-consuming tasks were the pre-processing steps i.e., masking of the photos, identification of reference points from the LiDAR DEM and then in the images, and processing of the images (the MVS step is particularly computationally intensive), which is directly related to the resolution and the number of photographs uploaded and the computer performance. Several steps required a certain degree of subjectivity, e.g., the identification of the GCPs. However, due to the high automatism of the image processing, the level of expertise is considerably lower than for LiDAR and traditional photogrammetry.

On the La Mare Glacier, the area-averaged estimates of the 2013-14 geodetic mass balance from ALS and photogrammetric data were almost identical (0.91 and 0.87 m w.e., respectively) and close to the mass balance calculated from the direct glaciological method (0.83 m w.e.). The differences are well within the uncertainty of the direct mass balance estimates, which was quantified in 0.26 m w.e. $y^{-1}$ by Carturan (2016). These results confirm that the good results obtained by Piermattei et al., (2015) on the small Montasio Glacier, in the Julian Alps, can also be replicated on larger glaciers with different morphologies and characteristics.

Because the AVDM3 Rock Glacier exhibited quite slow annual deformation and creep, we were able to calculate reliable displacement rates and area-averaged surface elevation changes only on a multi-year (in our case, decadal) time scale. This result confirms the findings of Gómez-Gutiérrez et al. (2014), who applied a similar method to the Corral del Veleta Rock Glacier in the Sierra Nevada (Spain).

Our results are promising, despite the limitations of the adopted method, which include i) the location of GCPs on natural targets outside the investigated glacier/rock

glacier, ii) the presence of areas with deep shadows and changes in the light during the survey, iii) the presence of fresh snow in the upper and middle part of the glacier, and iv) the high camera-object distance in the glacier application.

In general terms, the photo-based accuracy is related to the image feature extraction, feature matching (in both the SfM and MVS steps), and scale definition (Bemis et al., 2014). A low accuracy in these steps, caused for example by poor camera network geometry, can generate model distortion and reduce the ability to identify unique corresponding features in overlapping images (Wackrow and Chandler, 2011; Dall`Asta et al., 2015, Favalli et al., 2012; James and Robson, 2012; 2014; Hosseininaveh et al, 2014; Micheletti et al., 2014; Nocerino et al., 2014). In our case studies, among the various aspects analysed, the spatial variability of the accuracy of the photogrammetric DEMs is related to the camera-object distance, the presence of fresh snow with low contrast, the changing illumination during the survey and the occurrence of shadows. The increasing error with increasing terrain slope suggests the persistence of a small shift in the reconstructed DEMs. This shift, however does not affect the areal estimates of mass balance and elevation change, given that the vast majority of the glacier and rock glacier areas feature small or moderate slope angles. For both the glacier and the rock glacier, the spatial coverage of the reconstructed areas was not complete. In the glacier surveys, the problematic areas were those visible from a low number of camera positions and those covered by fresh snow and far from the viewpoints. In the rock glacier, certain areas were not reconstructed due to the rock glacier's complex morphology and in particular to the presence of ridges, furrows and counterslopes.

## 5.2 Possible improvements of the SfM-MVS approach

The accuracy assessments confirm that the ALS data still provide results with somewhat higher accuracies (Tabs. 3 and 5, Figs. 6 and 14) but with much higher costs and demanding logistics than the SfM-MVS approach. However, the SfM-MVS method has the potential to provide a significantly higher spatial resolution (Debella-Gilo and Kaab, 2011; Piermattei et al., 2015) and temporal resolution due to its significantly lower costs. Moreover, the photogrammetric reconstructions still have room for improvement, as demonstrated by the better results achieved from the 2014 survey of the glacier area compared to those from 2013. This improvement resulted from a higher number of photographs and improved camera network geometry.

Many of the limitations described above can be overcome by introducing modifications to the terrestrial photogrammetric survey strategy. For the rock glacier survey, shorter baselines are recommended to ensure greater spatial coverage, high image similarity and good matching performance (Wenzel et al., 2013). GCPs, for example, could be placed on the surface of the glaciers and rock glaciers to reduce the model distortions (Bemis et al., 2014) and generate surveys with much higher accuracies via, for example, the use of dGPS (Dall'Asta et al., 2015).

The use of UAVs could solve the problem of excessive camera-object distances and the issue of missing areas due to inaccessibility. However, these alternatives imply increased costs, more troublesome logistics, greater expertise, and ultimately longer survey times. In addition, they also require directly accessing unsafe or difficult to reach areas, both to place targets and to move UAVs among study areas that exceed their operational range (Bühler et al., 2014). Therefore, the best balance must be found between simplicity, safety, costs and accuracy for each photogrammetric application based on the final objectives and on the available human and economic resources.

## 6. Conclusions

In this paper, we investigated the applicability of the SfM-MVS approach for monitoring glacial and periglacial processes in a catchment of the Ortles-Cevedale Group (Eastern Italian Alps), validating our results using ALS DEMs as benchmarks. The ground surveys were conducted on foot and were intentionally planned to be as quick and easy as possible. The 2.1 $km^2$ La Mare Glacier and the neighbouring AVDM3 Rock Glacier were surveyed in one day using only a consumer-grade SLR camera without the setup of artificial targets.

The accuracy of the photogrammetric DEMs, evaluated as the mean and standard deviation of the elevation difference in a stable area between the SfM-MVS DEM and the reference ALS DEM, was -0.42 m ± 1.72 m and 0.03 m ± 0.74 m for the 2013 and 2014 surveys, respectively. The SfM-MVS DEM accuracy of the reconstructed rock glacier surface acquired in 2014 was estimated to be 0.02 m ± 0.17 m.

The SfM-MVS geodetic mass balance estimates for the La Mare Glacier were in good agreement with the calculations from the contemporary ALS data and with the results of the direct glaciological method, confirming a positive mass balance of

approximately 0.9 m w.e. in the 2013-14 hydrological year. In the rock glacier, the survey produced a good spatial coverage of the photogrammetric DEM and a reliable calculation of the multi-year surface changes and displacement rates. For rock glacier applications, particularly for slow-mowing ones such as AVDM3, single-year assessments of elevation change and surface velocities require the setup of artificial targets and GCPs to obtain the accuracy required to detect such slow processes.

The simplicity of the ground surveys and the physical characteristics of the analysed alpine terrain were the main factors influencing the tested approach. In particular, we refer to the use of natural targets as GCPs, the occurrence of shadowed areas and lighting changes during the surveys, the presence of fresh snow in the upper part of the glacier (which reduced the contrast), and the sub-optimal camera network geometry and long camera-object distances imposed by the morphology and accessibility of the study area. In consideration of the factors that spatially control the accuracy of the SfM-MVS DEMs, there remains room for significant improvements, e.g., using aerial platform and/or placing artificial targets surveyed by dGPS. Further research is therefore needed to i) find technical solutions to overcome the major limitations of the SfM-MVS approach in such remote areas and ii) achieve the optimal balance between the simplicity and low cost of this approach and the accuracy required for each specific application.

## Acknowledgments

This study was funded by the Italian MIUR Project (PRIN 2010-11): ‘Response of morphoclimatic system dynamics to global changes and related geomorphological hazards’ (local and national coordinators G. Dalla Fontana and C. Baroni). The authors would like to thank Philipp Glira from the TU of Wien for his precious contribution to the LiDAR data processing. The comments and suggestions from Susan Conway, Álvaro Gómez-Gutiérrez and an anonymous Reviewer have been useful for the improvement of the manuscript.

## References


AgiSoft LL C: AgiSoft PhotoScan Professional Edition. Version 1.1.2, available at: http://www.agisoft.ru/products/photoscan/ (last access: 18 January 2015), 2010a.

AgiSoft LL C: AgiSoft PhotoScan User-manuals Version 1.0, available at: http://www.agisoft.com/pdf/photoscan-pro_1_1_en.pdf (last access: 15 May 2015), 2010b.

Bemis, S., Micklethwaite, S., and Turner, D.: Ground-based and UAV-Based photogrammetry: a multi-scale, high-resolution mapping tool for Structural Geology and Paleoseismology. J Struct Geol., 69, 163–178, doi:10.1016/j.jsg.2014.10.007, 2014.

Bertone, A.: Misure di spostamento dei rock glacier con l'uso di feature tracking applicato a DTM multitemporali, BSc Thesis, Department of Earth and Environmental Sciences, University of Pavia, Pavia, Italy, 63 pp., 2014.

Besl, P. J. and McKay, N. D.: Method for registration of 3-D shapes, in: Proceedings of the International Society for Optics and Photonics IEEE Transactions on Pattern Analysis and Machine Intelligence, 1611, 586–606, 1992.

Bradley, D., Boubekeur, T., and Heidrich, W.: Accurate multi-view reconstruction using robust binocular stereo and surface meshing, in: IEEE Conference on Computer Vision and Pattern Recognition, Anchorage, AK, USA, 1–8, 2008.

Bühler, Y., Marty, M., Egli, L., Veitinger, J., Jonas, T., Thee, P., and Ginzler, C.: Spatially continuous mapping of snow depth in high alpine catchments using digital photogrammetry, The Cryosphere Discuss., 8, 3297–3333, doi:10.5194/tcd-8-3297-2014, 2014.

Carturan, L.: Climate change effects on the cryosphere and hydrology of a high-altitude watershed, PhD thesis, Department of Land, Environment, Agriculture and Forestry, University of Padova, Padova, Italy, 2010.

Carturan, L.: Replacing monitored glaciers undergoing extinction: a new measurement series on La Mare Glacier (Ortles-Cevedale, Italy), J. Glaciol., in review, 2016.

585 Carturan, L., Cazorzi, F., and Dalla Fontana, G.: Enhanced estimation of glacier
586 mass balance in unsampled areas by means of topographic data, Ann. Glaciol., 50,
587 37–46, 2009.

588 Carturan, L., Baldassi, G., Bondesan, A., Calligaro, S., Carton, A., Cazorzi, F., Dalla
589 Fontana, G., Francese, R., Guarnieri, A., Milan, N., Moro, D., Tarolli, P.: Current
590 behavior and dynamics of the lowermost italian glacier (Montasio Occidentale, Julian
591 Alps), Geografiska Annaler: Series A, Physical Geography, 95, 79–96, 2013.

592 Carturan, L., Baroni, C., Carton, A., Cazorzi, F., Fontana, G. D., Delpero, C., and
593 Zanoner, T.: Reconstructing Fluctuations of La Mare Glacier (Eastern Italian Alps) in
594 the Late Holocene: new Evidence for a Little Ice Age Maximum Around 1600 AD.
595 Geografiska Annaler: Series A, Physical Geography, 96, 287–306, 2014.

596 Carturan, L., Zuecco, G., Seppi, R., Zanoner, Z., Borga, M., Carton, A., and Dalla
597 Fontana, G.: Catchment-scale permafrost mapping using spring water
598 characteristics, Permafrost Periglac., in press, doi: 10.1002/ppp.1875, 2015.

599 Chen, Y. and Medioni, G.: Object modeling by registration of multiple range images,
600 in: Proceedings, IEEE International Conference on Robotics and Automation, 9–11
601 April, Sacramento, CA, USA, 10, 145–155, 1991.

602 Dall'Asta, E., Delaloye, R., Diotri, F., Forlani, G., Fornari, M., Morra di Cella, U.,
603 Pogliotti, P., Roncella, R., Santise, M.: Use of UAS in a high mountain landscape: the
604 case of gran sommetta rock glacier (AO), The International Archives of the
605 Photogrammetry, Remote Sensing and Spatial Information Sciences, Volume XL-
606 3/W3, 391–397, 2015a.

607 Debella-Gilo, M. and Kääb, A.: Sub-pixel precision image matching for measuring
608 surface displacements on mass movements using normalized cross-correlation.
609 Remote Sens. Environ., 115, 130–142, 2011.

610 Favalli, M., Fornaciai, A., Isola, I., Tarquini, S., and Nannipieri, L.: Multiview 3D
611 reconstruction in geosciences, Comput. Geosci., 44, 168–176, 2012.

612 Gauthier, D., Conlan, M., and Jamieson, B.: Photogrammetry of fracture lines and
613 avalanche terrain: potential applications to research and hazard mitigation projects,

614 Proceedings, International Snow Science Workshop, Banff, 29 September–3 October
615 2014, 109–115, 2014.

616 Glira, P., Pfeifer, N., Briese, C., Ressl, C.: A correspondence framework for ALS strip
617 adjustments based on variants of the ICP algorithm, Photogramm. Fernerkun., 4,
618 275–289, doi:10.1127/pfg/2015/0270, 2015.

619 Gómez-Gutiérrez, Á., de Sanjosé-Blasco, J. J., de Matías-Bejarano, J., and
620 Berenguer-Sempere, F.: Comparing two photo-reconstruction methods to produce
621 high density point clouds and DEMs in the Corral del Veleta Rock Glacier (Sierra
622 Nevada, Spain), Remote Sensing, 6, 5407–5427, 2014.

623 Gómez-Gutiérrez, Á., de Sanjosé-Blasco, J. J., Lozano-Parra, J., Berenguer-
624 Sempere, F., and de Matías-Bejarano, J.: Does HDR pre-processing improve the
625 accuracy of 3D models obtained by means of two conventional SfM-MVS software
626 packages? The case of the Corral del Veleta Rock Glacier, Remote Sensing, 7,
627 10269–10294, 2015.

628 Hartley, R. and Zisserman, A.: Multiple View Geometry, In Computer Vision,
629 Cambridge University Press, Cambridge, UK, 2003.

630 Haeberli, W.: Creep of mountain permafrost: internal structure and flow of alpine rock
631 glaciers, Mitteilungen der Versuchsanstalt für Wasserbau, Hydrologie und Glaziologie
632 der ETH Zurich, 77, 5–142, 1985.

633 Hosseininaveh, A., Sargeant, B., Erfani, T., Robson, S., Shortis, M., Hess, M., and
634 Boehm, J.: Towards fully automatic reliable 3D acquisition: from designing imaging
635 network to a complete and accurate point cloud, Robotics and Autonomous Systems,
636 62, 1197–1207, 2014.

637 Huss, M.: Density assumptions for converting geodetic glacier volume change to
638 mass change, The Cryosphere, 7, 877-887, doi:10.5194/tc-7-877-2013, 2013.

639 Immerzeel, W. W., Kraaijenbrink, P. D. A., Shea, J. M., Shrestha, A. B., Pellicciotti,
640 F., Bierkens, M. F. P., and De Jong, S. M.: High-resolution monitoring of Himalayan
641 glacier dynamics using unmanned aerial vehicles, Remote Sens. Environ., 150, 93–
642 103, 2014.

643 Isaksen, K., Ødegård, R. S., Eiken, T., and Sollid, J. L.: Composition, flow and
644 development of two tongue-shaped rock glaciers in the permafrost of Svalbard.
645 Permafrost and Periglacial Processes, 11, 241-257, 2000.

646 James, M. R. and Robson, S.: Straightforward reconstruction of 3D surfaces and
647 topography with a camera: accuracy and geoscience application, J. Geophys. Res.-
648 Earth, 117, F03017, doi:10.1029/2011JF002289, 2012.

649 James, M. R. and Robson, S.: Mitigating systematic error in topographic models
650 derived from UAV and ground-based image networks, Earth Surf. Proc. Land. 39,
651 1413–1420, doi:10.1002/esp.3609, 2014.

652 Kääb, A.: Monitoring high-mountain terrain deformation from repeated air-and
653 spaceborne optical data: examples using digital aerial imagery and ASTER data.
654 ISPRS Journal of Photogrammetry and remote sensing, 57, 39–52, 2002.

655 Kääb, A.: Remote Sensing of Mountain Glaciers and Permafrost Creep. Research
656 Perspectives from Earth Observation Technologies and Geoinformatics,
657 Schriftenreihe Physische Geographie, Glaziologie und Geomorphodynamik, 48,
658 University of Zurich, Zurich, Switzerland, 2005.

659 Kääb, A., Kaufmann, V., Ladstädter, R., and Eiken, T.: Rock glacier dynamics:
660 implications from high-resolution measurements of surface velocity fields, in: Eighth
661 International Conference on Permafrost, 21–25 July 2003, Zurich, Switzerland, Vol.
662 1, 501–506, 2003.

663 Kääb, A., Girod, L., and Berthling, I.: Surface kinematics of periglacial sorted circles
664 using structure-from-motion technology, The Cryosphere, 8, 1041–1056,
665 doi:10.5194/tc-8-1041-2014, 2014.

666 Micheletti, N., Chandler, J. H., and Lane, S. N.: Investigating the geomorphological
667 potential of freely available and accessible Structure-from-Motion photogrammetry
668 using a smartphone, Earth Surf. Proc. Land., 40, 473–486, doi:10.1002/esp.3648,
669 2014.

670 Nilosek, D., Sun, S., and Salvaggio, C.: Geo-accurate model extraction from three-
671 dimensional image-derived point clouds, in: Proceedings of SPIE, Algorithms and

672 Technologies for Multispectral, Hyperspectral, and Ultraspectral Imagery XVIII, 23
673 April 2012, Baltimore, MD, USA, 8390, 83900J, doi:10.1117/12.919148, 2012.

674 Nocerino, E., Menna, F., and Remondino, F.: Accuracy of typical photogrammetric
675 networks in cultural heritage 3D modeling projects, ISPRS-International Archives of
676 the Photogrammetry, Remote Sensing and Spatial Information Sciences, 1, 465–472,
677 2014.

678 Piermattei, L., Carturan, L., and Guarnieri, A.: Use of terrestrial photogrammetry
679 based on structure from motion for mass balance estimation of a small glacier in the
680 Italian Alps, Earth Surf. Proc. Land., 40, 1791–1802, doi:10.1002/esp.3756, 2015.

681 Ryan, J. C., Hubbard, A. L., Box, J. E., Todd, J., Christoffersen, P., Carr, J. R., Holt,
682 T. O., and Snooke, N.: UAV photogrammetry and structure from motion to assess
683 calving dynamics at Store Glacier, a large outlet draining the Greenland ice sheet,
684 The Cryosphere, 9, 1–11, doi:10.5194/tc-9-1-2015, 2015.

685 Roer, I. and Nyenhuis, M.: Rockglacier activity studies on a regional scale:
686 comparison of geomorphological mapping and photogrammetric monitoring, Earth
687 Surf. Proc. Land., 32, 1747–1758, 2007.

688 Seppi, R., Carton, A., Zumiani, M., Dall'Amico, M., Zampedri, G., and Rigon, R.:
689 Inventory, distribution and topographic features of rock glaciers in the southern region
690 of the Eastern Italian Alps (Trentino). Geografia Fisica e Dinamica Quaternaria 35,
691 185–197, doi:10.4461/GFDQ.2012.35.17, 2012.

692 Solbø, S. and Storvold, R.: Mapping svalbard glaciers with the cryowing uas, ISPRS
693 International Archives of the Photogrammetry, Remote Sensing and Spatial
694 Information Sciences, XL-1/W2, 373–377, 2013.

695 Tonkin, T. N., Midgley, N. G., Graham, D. J., and Labadz, J. C.: The potential of
696 small unmanned aircraft systems and structure-from-motion for topographic surveys:
697 a test of emerging integrated approaches at Cwm Idwal, North Wales,
698 Geomorphology, 226, 35–43, 2014.

699 Tseng, C.-M., Lin, C. W., Dalla Fontana, G., Tarolli, P.: The topographic signature of
700 a Major Typhoon, Earth Surf. Proc. Land., 40, 1129–1136, 2015.

Verhoeven, G., Karel, W., ’tuhec, S., Doneus, M., Trinks, I., and Pfeifer, N.: Mind your grey tones – examining the influence of decolourization methods on interest point extraction and matching for architectural image-based modelling, in: 3D-Arch 2015–3D Virtual Reconstruction and Visualization of Complex Architectures (ISPRS WG V/4, CIPA), 25–27 February 2015, Vol. 40, ISPRS, Avila, Spain, 307–314, 2015.

Wackrow, R. and Chandler, J.: Minimising systematic error surfaces in digital elevation models using oblique convergent imagery, Photogramm. Rec., 26, 16–31, 2011.

Wenzel, K., Rothermel, M., Fritsch, D., and Haala, N.: Image acquisition and model selection for multi-view stereo, Int. Arch. Photogramm. Remote Sens. Spatial Inf. Sci, 251–258, 2013.

Whitehead, K., Moorman, B. J., and Hugenholtz, C. H.: Brief Communication: Low-cost, ondemand aerial photogrammetry for glaciological measurement, The Cryosphere, 7, 1879–1884, doi:10.5194/tc-7-1879-2013, 2013.

Zemp, M., Thibert, E., Huss, M., Stumm, D., Denby, C. R., Nuth, C., Nussbaumer, S. U., Moholdt, G., Mercer, A., Mayer, C., Joerg, P. C., Jansson, P., Hynek, B., Fischer, A., Escher-Vetter, H., Elvehøy, H., and Andreassen, L. M.: Reanalysing glacier mass balance measurement series. The Cryosphere, 7, 1227-1245, doi:10.5194/tc-7-1227-2013, 2013.

729 **Table 1**. Date and main parameters of available LiDAR data.

| Date | Aircraft | Laser scanner model | Laser scanner rate | Max. scan angle | Scan frequency | Point density [pts·m$^{-2}$] |
|---|---|---|---|---|---|---|
| 24 Sept. 2014 | Elicopter AS350 B3 | Optech ALTM GEMINI (04SEN164) | 100 kHz | 46° | 34 Hz | 5.1 |
| 22 Sept. 2013 | Cessna 404 D-IDOS | ALTM 3100 | 70,000 Hz | ±25° | 32 Hz | 0.9 |
| 17 Sept. 2003 | — | — | — | — | — | 0.5 |

730

731 **Table 2**. Data acquisition settings and processing results of the photogrammetric
732 surveys for both case studies. The GCPs error is the average transformation
733 residuals error [m] and root mean square reprojection error for the GCPs [pix] during
734 the bundle adjustment computation. The image quality represents the downsized of
735 the images resolution during the dense matching computation. “Ultra high” means full
736 resolution, “High” a downsized of 50% before the image matching processing. The
737 ground sample distance (GSD) is the average pixel size on the ground. The standard
738 deviation of ICP registration is reported in the table.

| | **La Mare glacier** | | **Rock glacier** |
|---|---|---|---|
| | 4 September 2013 | 27 September 2014 | 27 September 2014 |
| *Input data* | | | |
| Camera type | Nikon 600D | Nikon 600D | Canon 5D Mark III |
| Focal Length | 25 mm | 35 mm | 28 mm |
| Image size | 5184 x 3456 pix | 5184 x 3456 pix | 5760 x 3840 pix |
| N° Images | 37 | 177 | 198 |
| *Processing data* | | | |
| Reprojection error | 0.43 pix (1.76 max) | 0.40 pix (3.75 max) | 0.38 pix (1.20 max) |
| GCPs error | 1.52 m 1.48 pix | 1.14 m 1.96 pix | 0.62 m 1.86 pix |
| Image quality | Ultra high | High | High |
| Mean GSD | 0.16 m/pix | 0.22 m/pix | 0.064 m/pix |
| Dense point cloud | 49,844,094 pts | 55,114,074 pts | 56,171,705 pts |
| Point density | 37 pts m$^{-2}$ | 20 pts m$^{-2}$ | 244 pts m$^{-2}$ |
| *Post-processing data* | | | |
| Filtered point cloud /subsampled | 15,617,342 pts (sampled 0.20 m) | 24,226,221 pts (sampled 0.20 m) | 4,517,143 pts (sampled 0.10 m) |
| Point density | 8 pts m$^{-2}$ | 9 pts m$^{-2}$ | 21 pts m$^{-2}$ |
| ICP transformation | 0.14 m | 0.15 m | 0.10 m |

739

740

741

742 **Table 3**. Results of comparisons between SfM-MVS-based DEMs vs. ALS-based
743 DEMs in the common area and for the bare-ground stable area and glacier.

| DEMs | Elevation differences [m] cell size 1 m x 1m | | | | | | | |
|---|---|---|---|---|---|---|---|---|
| | Common SfM-MVS bare-ground area | | | | Common SfM-MVS glacier area | | | |
| | *Min* | *Max* | *Mean* | *σ* | *Min* | *Max* | *Mean* | *σ* |
| SfM-MVS 2013 - ALS 2013 | -19.59 | 33.61 | -0.42 | 1.72 | -9.91 | 12.04 | -0.13 | 0.78 |
| SfM-MVS 2014 - ALS 2014 | -18.48 | 22.42 | 0.03 | 0.74 | -18.17 | 11.41 | 0.23 | 0.65 |
| SfM-MVS 2014 - SfM-MVS 2013 | -33.12 | 14.19 | 0.38 | 1.73 | -12.44 | 12.33 | 1.58 | 1.42 |
| ALS 2014 - ALS 2013 | -15.38 | 10.81 | -0.09 | 0.29 | -14.61 | 7.37 | 1.30 | 0.97 |

744

745 **Table 4.** Mass balance calculations on La Mare Glaciers using different combinations
746 of SfM-MVS and ALS DEMs.

| DEMs cell size 10 m | Mass balance estimation | | | | | | | |
|---|---|---|---|---|---|---|---|---|
| | Spatial coverage [$m^2$] | Average elevation changes [m] | | Volume change [$m^3$] | | Mass balance [m w.e] | |
| | | *Raw* | *Corrected* | *Raw* | *Corrected* | *Raw* | *Corrected* |
| SfM-MVS 2014 - SfM-MVS 2013 | 1,834,800 (~88%) | 1.81 | 1.45 | 3,320,988 | 2,660,460 | 1.09 | 0.87 |
| ALS 2014 - ALS 2013 | | 1.47 | 1.56 | 2,697,156 | 2,862,288 | 0.88 | 0.94 |
| SfM-MVS 2014 - ALS 2013 | 1,938,700 (~93%) | 1.64 | 1.70 | 3,179,468 | 3,295,790 | 0.98 | 1.02 |
| ALS 2014 - ALS 2013 | | 1.41 | 1.50 | 2,733,567 | 2,908,050 | 0.85 | 0.90 |
| ALS 2014 - ALS 2013 | 2,072,700 (entire glacier) | 1.43 | 1.52 | 2,963,961 | 3,150,504 | 0.86 | 0.91 |

747
748
749
750
751
752
753
754
755
756
757

**Table 5.** Statistics of elevation changes in the rock glacier and in bare ground stable area off rock glacier from September 2014 to September 2013 and September 2003 in the ALS reconstructed area and in the common ALS and SfM-MVS coverage area.

| Elevation changes [m] | | | | | | | | | |
|---|---|---|---|---|---|---|---|---|---|
| Data | | | ALS Reconstructed area | | | | SfM-MVS Reconstructed area | | | |
| | | | Stable area | | Rock glacier | | Stable area | | Rock glacier | |
| | | | *Mean* | *σ* | *Mean* | *σ* | *Mean* | *σ* | *Mean* | *σ* |
| SfM 2014 | - | ALS 2014 | — | — | — | — | 0.05 | 0.31 | 0.02 | 0.17 |
| SfM 2014 | - | ALS 2013 | — | — | — | — | 0.01 | 0.33 | -0.04 | 0.18 |
| ALS 2014 | - | ALS 2013 | -0.05 | 0.19 | -0.07 | 0.12 | -0.05 | 0.20 | -0.07 | 0.12 |
| SfM 2014 | - | ALS 2003 | — | — | — | — | 0.06 | 0.33 | -0.16 | 0.49 |
| ALS 2014 | - | ALS 2003 | -0.01 | 0.22 | -0.18 | 0.46 | -0.00 | 0.21 | -0.18 | 0.47 |
| ALS 2013 | - | ALS 2003 | 0.04 | 0.21 | -0.11 | 0.41 | — | — | — | — |

**Table 6**. Velocity statistics in three distinct areas of the rock glacier and in stable area outside the rock glacier evaluated comparing the 2003 and 2014 ALS DEMs and the photogrammetric DEM for the 2014 survey epoch.

| Horizontal movements between 2003 and 2014 [cm yr $^{-1}$] | | | | | | | | | | |
|---|---|---|---|---|---|---|---|---|---|---|
| | ALS 2003 - ALS 2014 | | | | | ALS 2003 - SfM-MVS 2014 | | | | |
| | *No. points* | *Min* | *Max* | *Mean* | *σ* | *No. points* | *Min* | *Max* | *Mean* | *σ* |
| Area 1 | 41 | 7.3 | 43.3 | 26.8 | 8.9 | 36 | 6.8 | 47.5 | 26.3 | 10.3 |
| Area 2 | 13 | 4.4 | 27.4 | 18.9 | 7.0 | 11 | 9.0 | 27.9 | 18.1 | 6.4 |
| Area 3 | 26 | 4.5 | 16.5 | 9.4 | 4.0 | 24 | 4.5 | 18.2 | 9.0 | 4.1 |
| Off rock glacier | 65 | 0.0 | 10.7 | 3.6 | 3.1 | 23 | 0.0 | 13.6 | 5.3 | 4.2 |

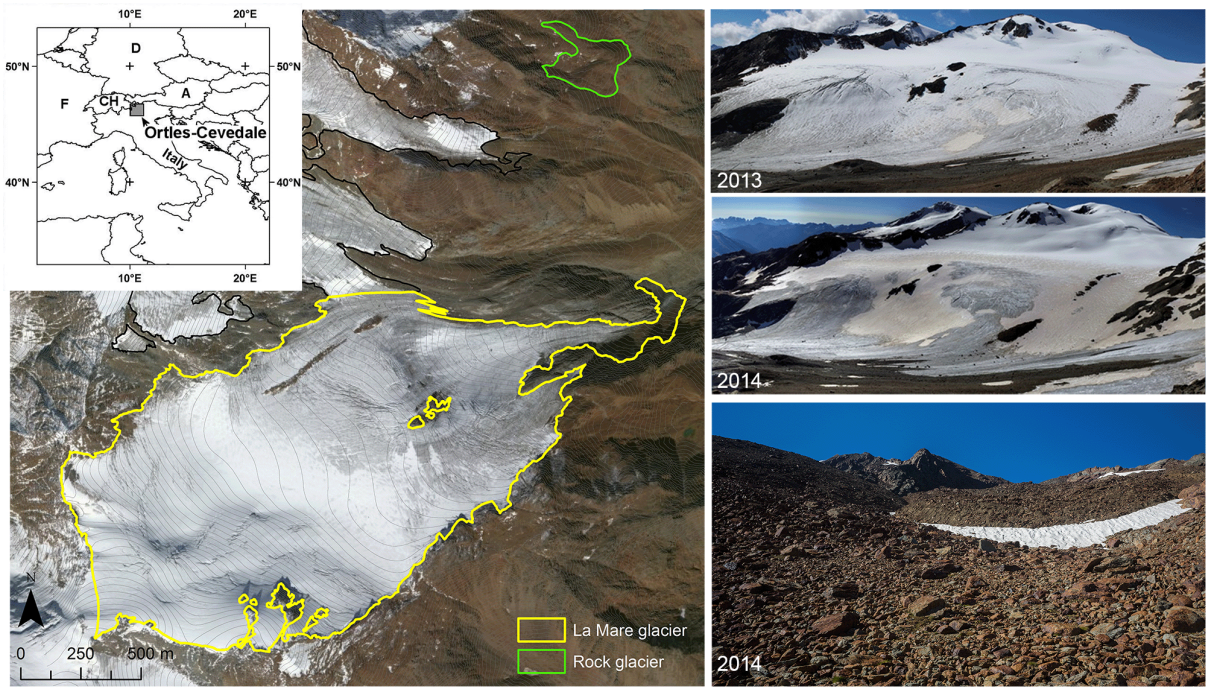


**Figure 1**. Geographic setting of study areas. Panorama view of the La Mare Glacier from the same camera position on 4 September 2013 and 27 September 2014. The lower right photograph shows the front of the meridional lobe of the AVDM3 Rock Glacier, which was surveyed on 27 September 2014.

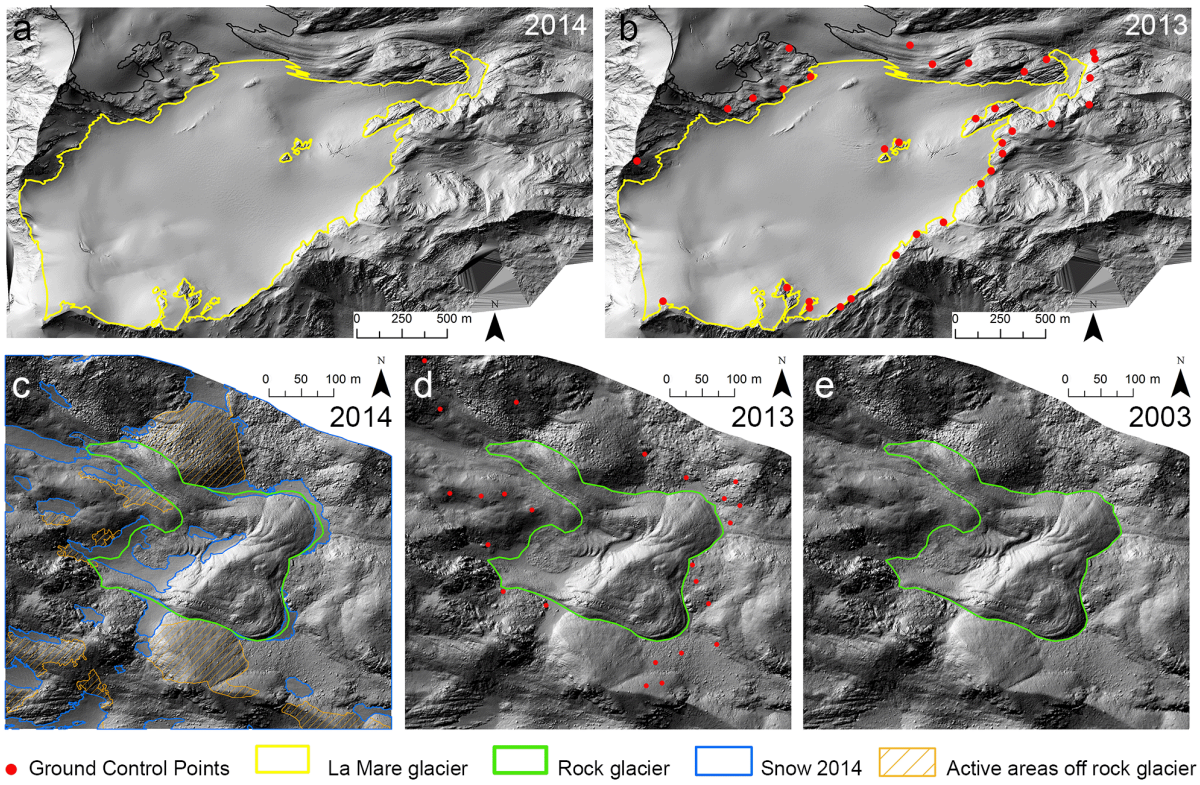


**Figure 2**. ALS shade DEMs of la Mare glacier acquired on **(a)** September 24, 2014 and **(b)** September 21, 2013. The ALS DEMs of rock glacier acquired on **(c)** 2014, **(d)** 2013 and **(e)** 2003.The red dots represent the selected GCPs in 2013 DEM used in the photogrammetric approach. The snow accumulation areas and geomorphologically-active areas outside the rock glacier were excluded during the ICP computation between 2013 and 2003, 2014 ALS point cloud.

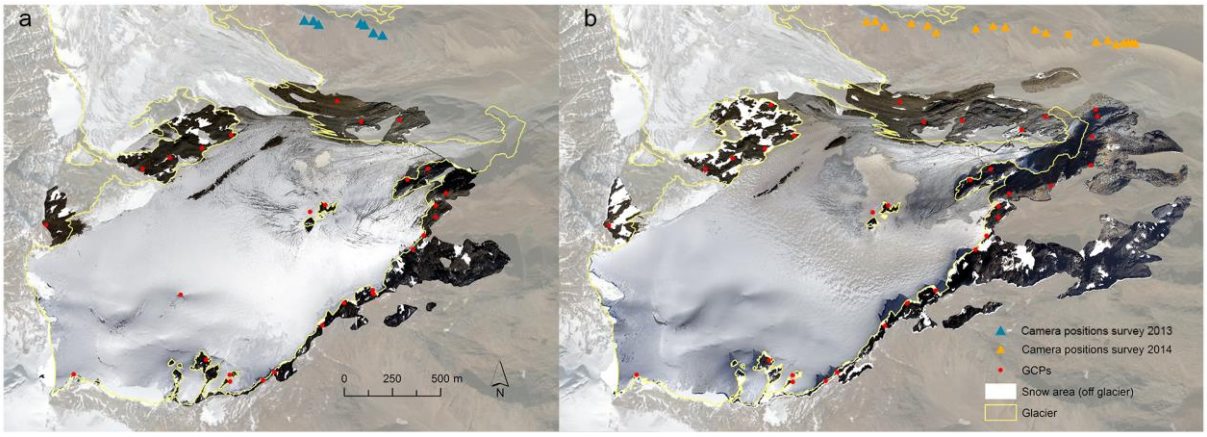


**Figure 3**. Orthophoto-images of SfM-MVS 3D model of La Mare glacier surveyed on **(a)** 4 September 2013 and **(b)** 27 September 2014. The white areas in the ortho-images represent the snow-covered area in the rock stable area. The red dots outside the glacier area are the GCPs and the triangles identified the camera locations.

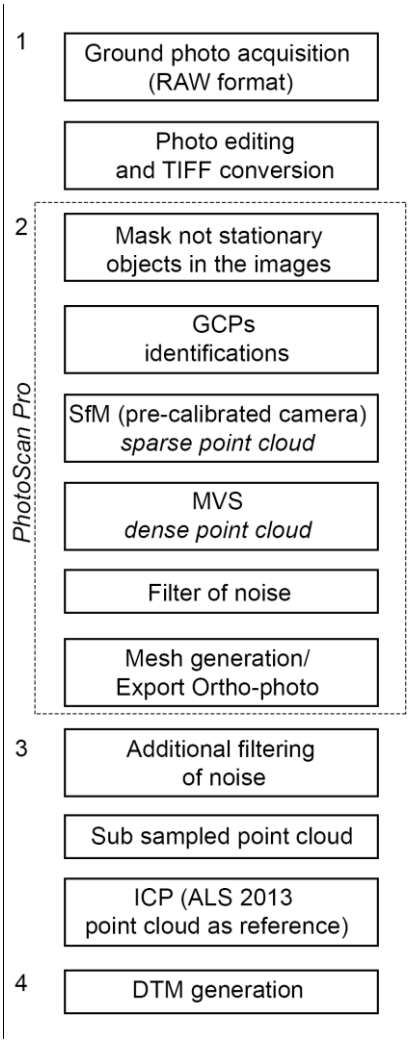


**Figure 4**. Workflow illustrating the photo-based 3D reconstruction process used in this work for both case studies, starting from images collection to DEM generation.

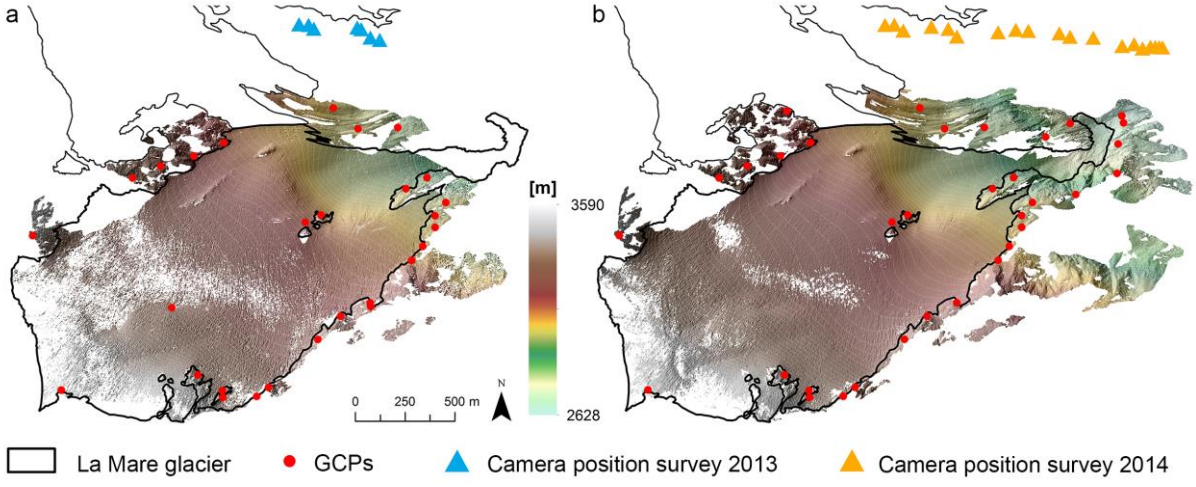


**Figure 5**. Hillshaded DEMs of La Mare glacier derived from photogrammetric measurements on **(a)** 4 September 2013 and **(b)** 27 September 2014.

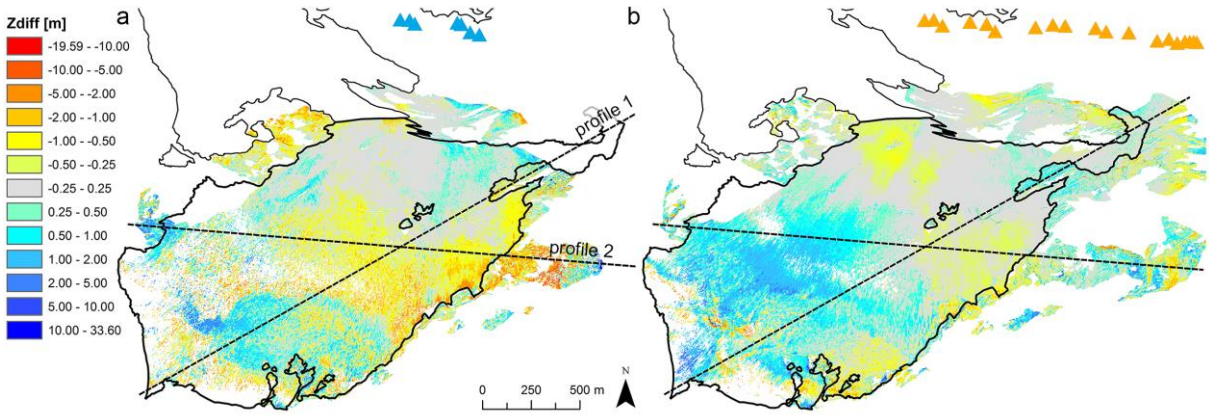


**Figure 6**. Spatial distribution of elevation differences between photogrammetric and ALS-based DEMs on **(a)** 2013 and **(b)** 2014.

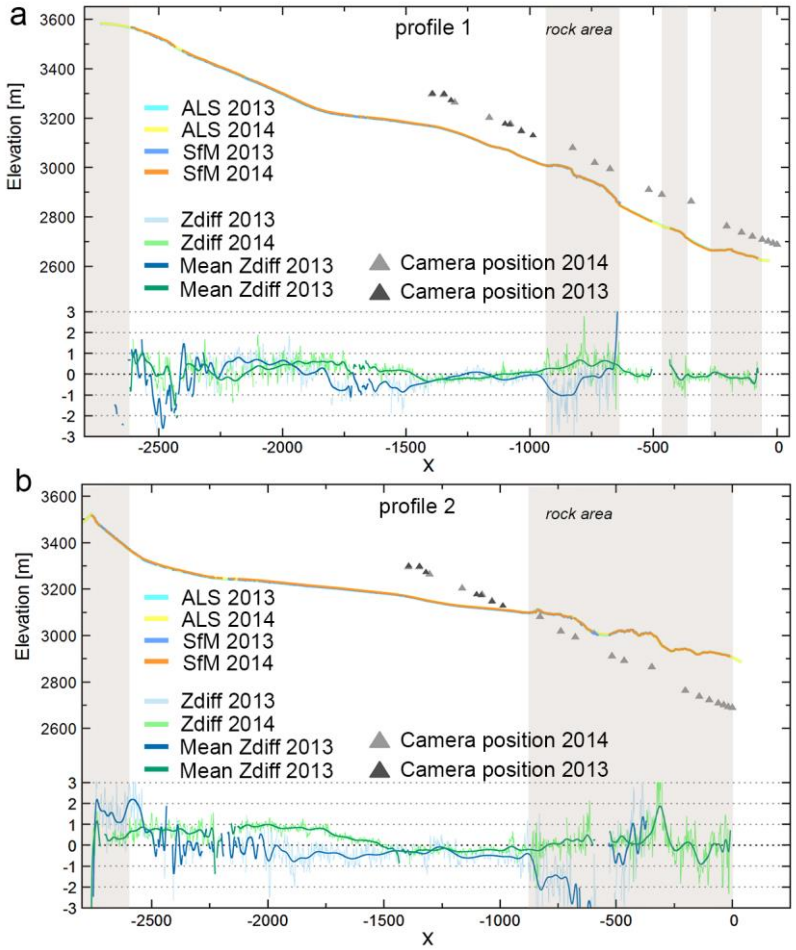


**Figure 7**. Cross sections through the La Mare glacier DEMs show the glacier elevation change and the difference between 2013 and 2014 in SfM-MVS and ALS-based DEMs. The location of **(a)** the profile 1 and **(b)** profile 2 is indicated in Fig. 6. The x-axis zero has been fixed at the first camera position of the 2014 survey and the minimum and maximum values of the z-difference set to ± 3 m and both profiles and the camera positions were projected onto the xz-plan.

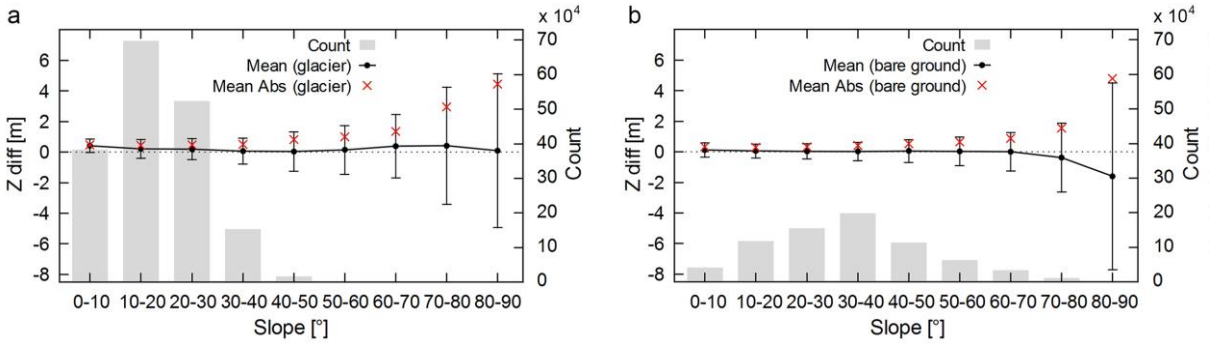


**Figure 8**. Mean, mean of the absolute values and standard deviation of the 2014 DoD between SfM-MVS and ALS-based DEM depending on slope calculated **(a)** in the glacier area and **(b)** in the bare ground outside glacier covered by rock. The grey bars show the count of cells at any given slope (y-axis on the right).

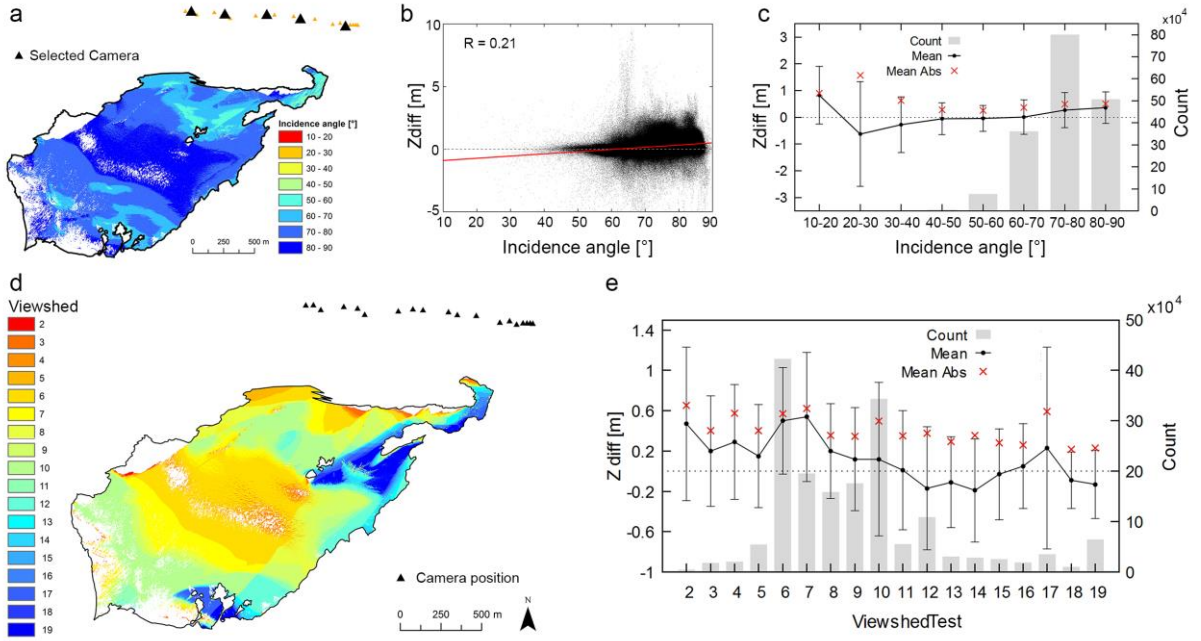


**Figure 9**. Mean incidence angles between five cameras positions and vectors normal to the surface and viewshed analysis. **(a)** Map of the mean incidence angle calculated for five representative camera positions; **(b)** the scatterplot of the elevation difference and the mean incidence angle for the five camera positions; **(c)** mean with one standard deviation y bars and mean of the absolute value of elevation differences for the mean incidence angle intervals calculated for 5 selected camera; **(d)** map of the viewshed reconstructed area visible from all camera; **(e)** mean with one standard deviation y bars and mean of the absolute value of elevation differences for the viewshed reconstructed area.

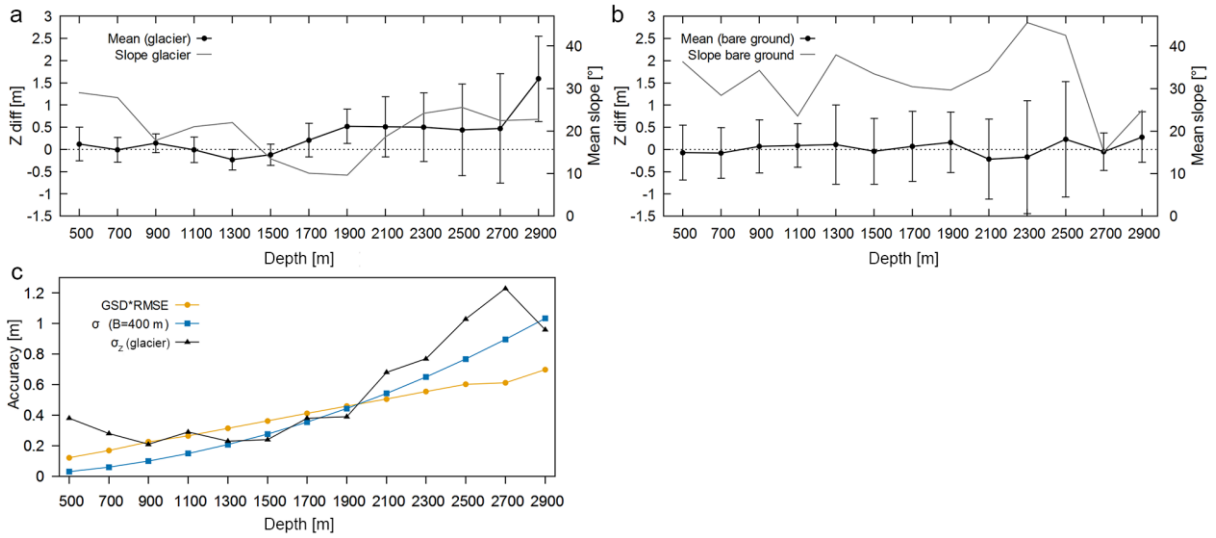


**Figure 10**. Mean and standard deviation of the 2014 DoD between SfM-MVS and ALS-based DEM depending on depth calculated **(a)** in the glacier area and **(b)** in the bare ground outside glacier covered by rock. The trend of the average slope angle for depth intervals is shown on the right y-axis. **(c)** Comparison of $\sigma_z$ measured in the glacier reconstructed area, the theoretical depth accuracy estimated according to the Eq. (1) and the GSD multiplied for the GCPs RMSE for the depth intervals.

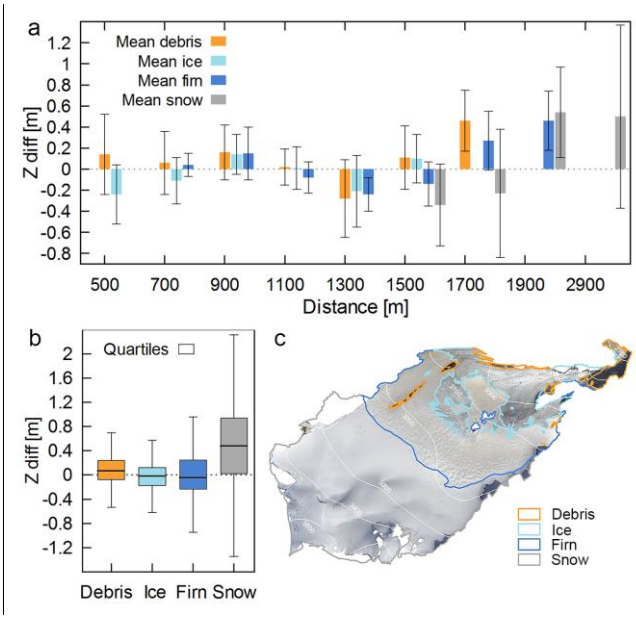


**Figure 11**. Elevation difference between the 2014 SfM-MVS and ALS-based DEMs calculated for different substrata. The figure shows **(a)** the mean and standard deviation of z-difference for four substrata (debris, ice, firn, and snow) grouped by distance from camera position; **(b)** the box plot of the z-difference for four substrata. In the box-whisker plot, values which exceed 1.5 * IQR were considered outliers. In panel **(c)** the orthophoto of the glacier on 27 September 2014 and map of substrata.

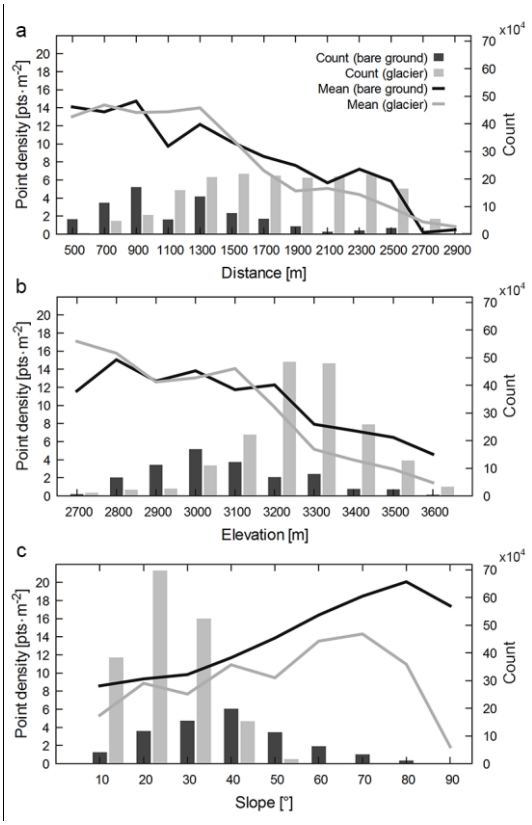


**Figure 12**. Relationships between point density of the 2014 photogrammetric 3D model and **(a)** camera-object distance, **(b)** elevation and **(c)** slope calculated for the glacier and rock stable area outside glacier. The point density was estimated using the filtered and subsampled point cloud.

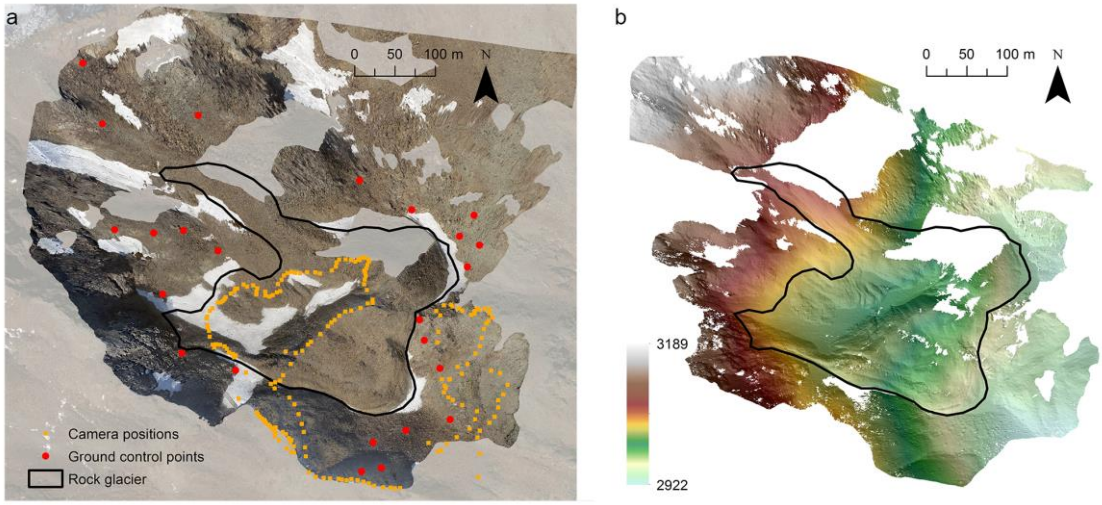


**Figure 13**. Correspondence between **(a)** the orthophoto of SfM-MVS 3D model of rock glacier surveyed on 27 September 2014 and **(b)** the hillshade model of rock glacier model calculated at the same data and hour of the images acquisition. The holes in the DEM represent not reconstructed area.

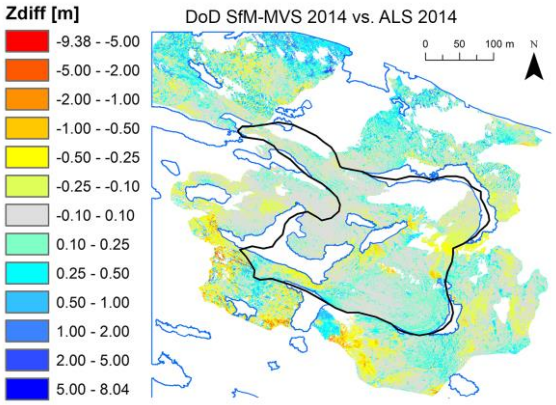


**Figure 14**. Spatial distribution of elevation differences between photogrammetric and ALS-based DEM acquired on 27 September 2014 and 24 September 2014, respectively. The blue shape is the snow accumulation areas excluded during the DEMs comparison.

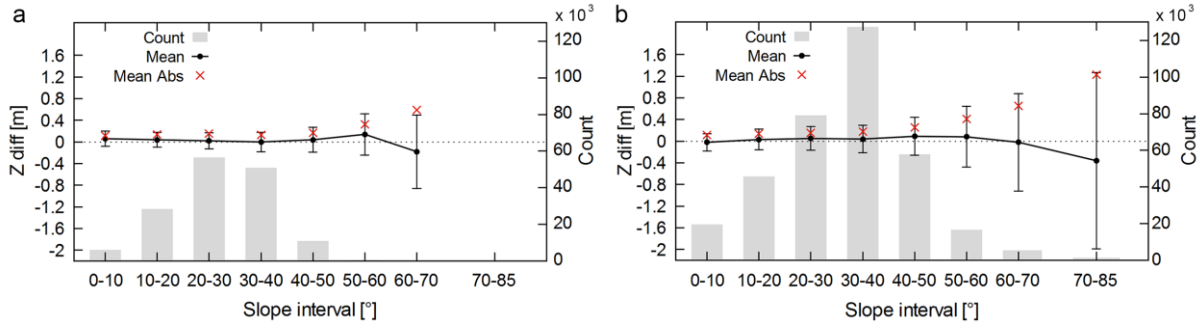


**Figure 15**. Mean, mean of the absolute values and standard deviation of elevation differences between 2014 SfM-MVS and ALS-based DEMs calculated for the slope interval **(a)** in the rock glacier reconstructed area and **(b)** in the bare ground outside the rock glacier.

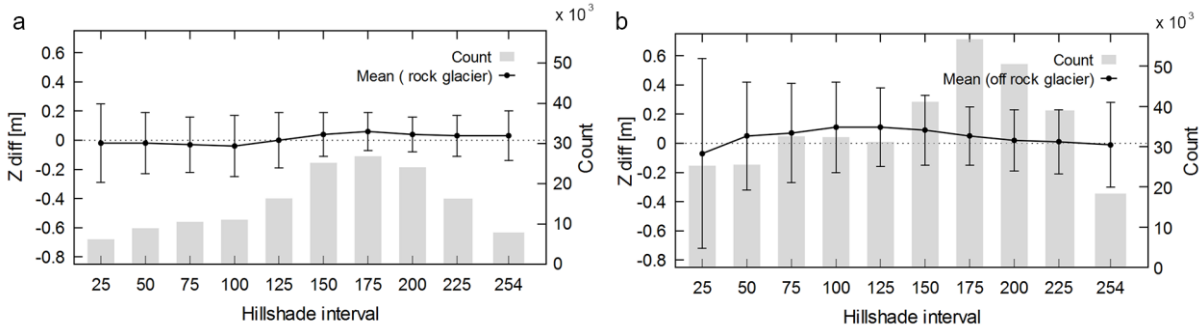


**Figure 16**. Elevation differences between 2014 SfM-MVS and ALS-based DEMs calculated for the hillshade interval **(a)** in the rock glacier reconstructed area and **(b)** in the bare ground outside the rock glacier. Lowest values represent shadowed area whilst lighted areas present the highest values.

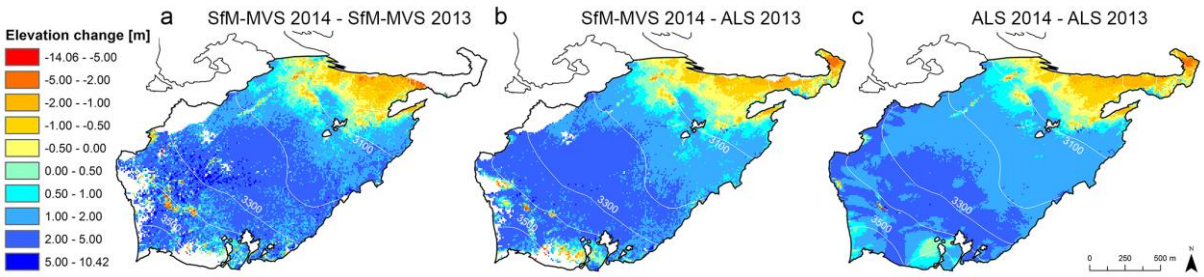


**Figure 17**. Spatial distribution of elevation changes between **(a)** SfM-MVS 2014 and SfM-MVS 2013 DEMs **(b)** SfM-MVS 2014 and ALS 2013 over the area of the glacier with common coverage and **(c)** ALS 2014 and ALS 2013 over the entire glacier.

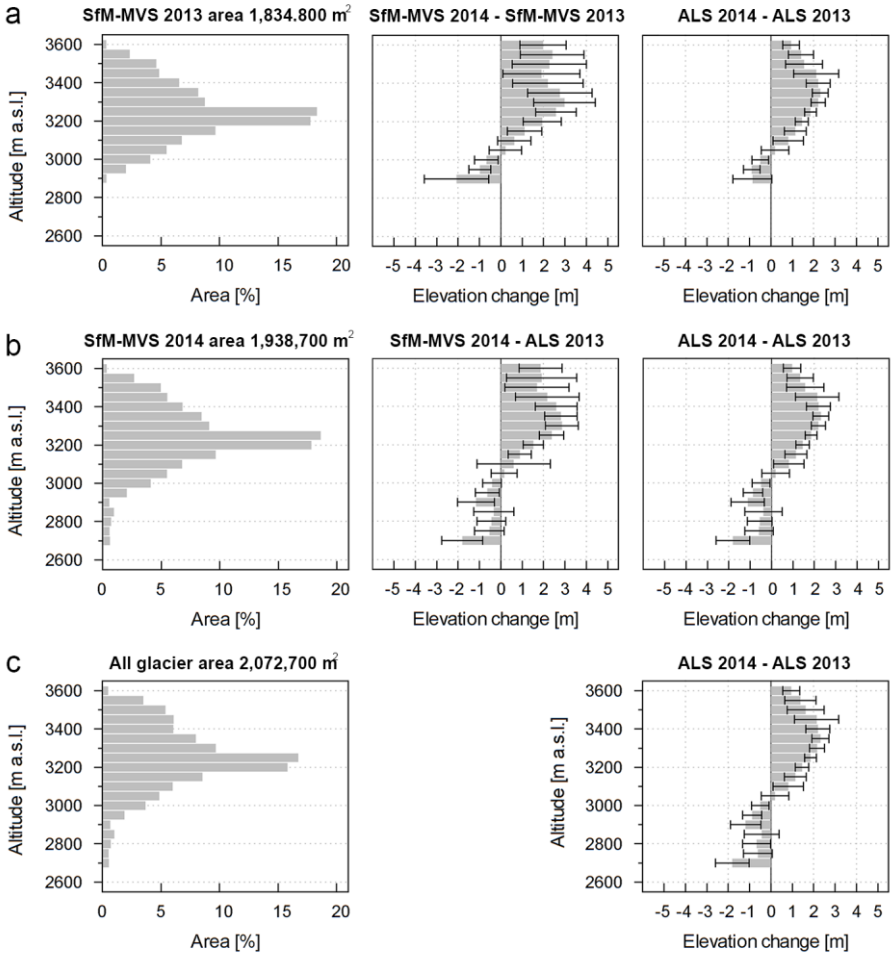


**Figure 18**. Area-altitude distribution and surface elevation change with standard deviation for the glaciological year 2014/2013 displayed for altitudinal bands with 50 m interval. The elevation change were calculated between **(a)** SfM-MVS DEMs of 2013 and 2014 in the 2013 photogrammetric reconstructed area; **(b)** SfM-MVS DEMs of2014 and ALS DEM of 2014 in the 2014 photogrammetric reconstructed area; **(c)** ALS DEMs of 2013 and 2014 of the entire glacier. The photogrammetric results were compared with the corresponding ALS result calculated in the same area.

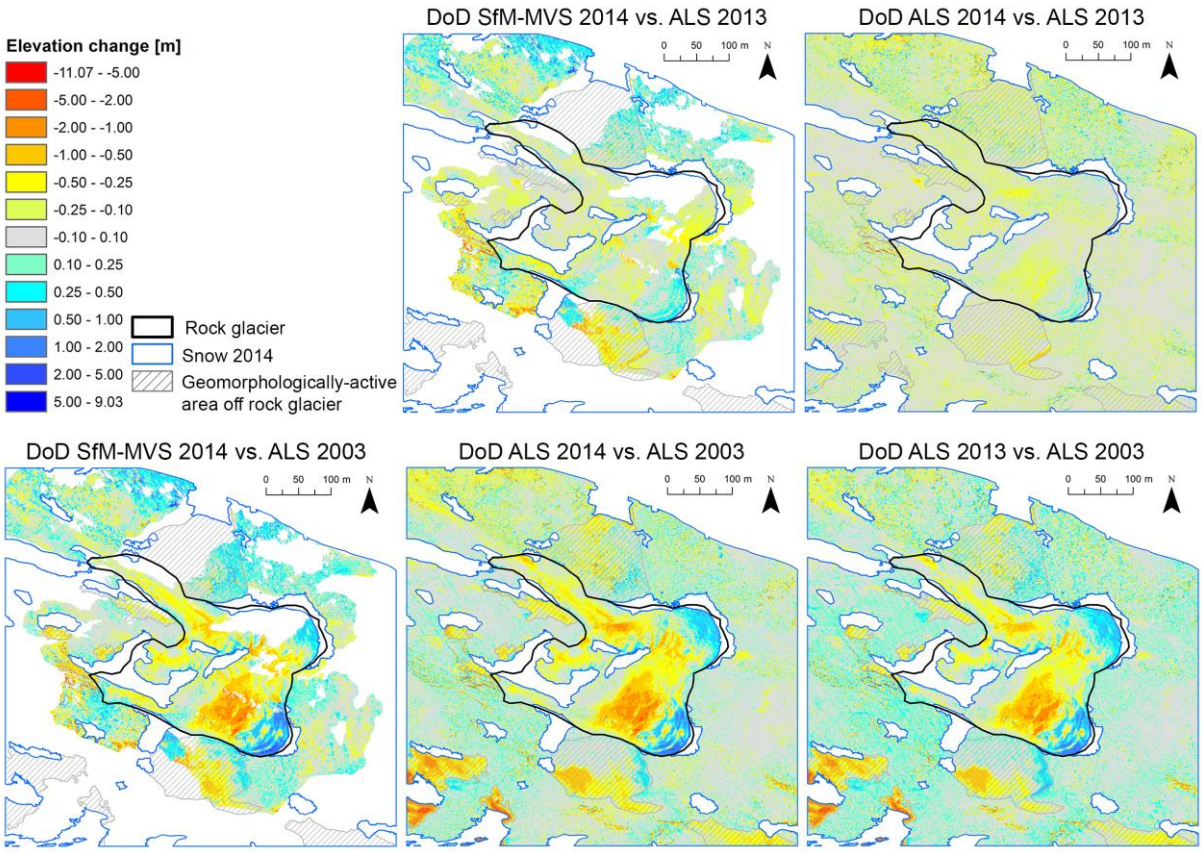


875

876 **Figure 19**. Spatial distribution of elevation changes from September 2014 to
877 September 2013 and September 2003 between the DEMs derived from SfM-MVS
878 and ALS.

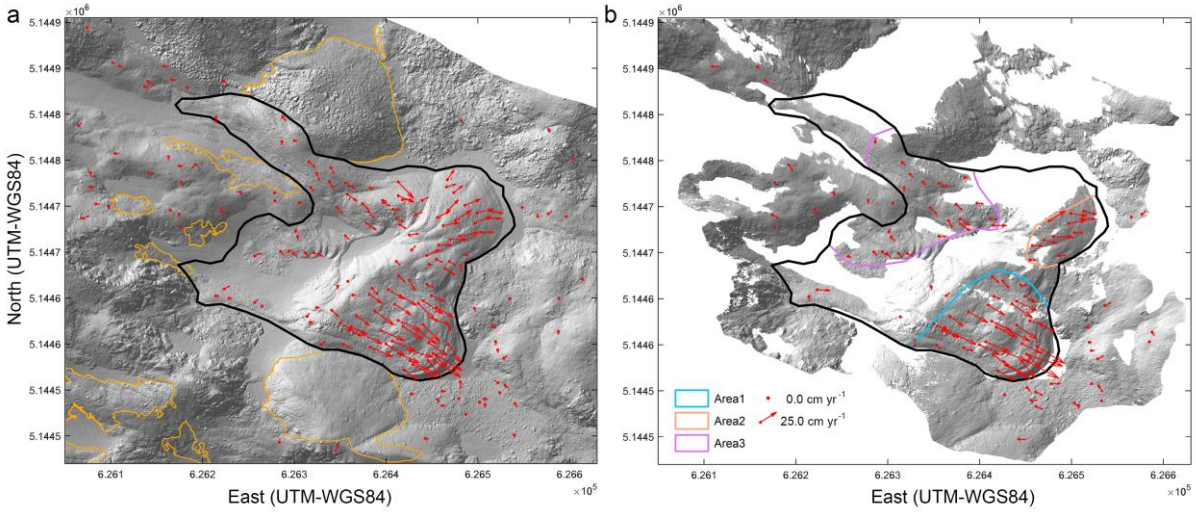


879

880 **Figure 20**. Displacement vectors of the rock glacier between 2003 and 2014
881 computed by a manual identification of natural features visible in the shaded DEMs
882 generated by **(a)** ALS for both survey epochs and by **(b)** ALS and photogrammetry
883 for 2003 and 2014 survey, respectively.